Generalization of helicoidal beams for short pulses

Jean-Louis Thomas, T. Brunet, F. Coulouvrat

Generalization of helicoidal beams for short pulses

Jean-Louis Thomas[1], Thomas Brunet[1,2], and François Coulouvrat[2]
[1] *CNRS, Université Pierre et Marie Curie - Paris 6, UMR 7588, Institut des NanoSciences de Paris, 140 rue de Lourmel, Paris, F-75015 France and*
[2] *Université Pierre et Marie Curie - Paris 6, CNRS, UMR 7190, Institut Jean le Rond d'Alembert, 4 place Jussieu, Paris, F-75005 France*
(Dated: December 7, 2010)

A generalization to the transient regime is developed for waves with a phase singularity of the screw type. These singular waves are commonly called vortices for all kind of waves as for instance, optical vortex or acoustical vortex. We generalize the definition of vortices to get an azimuthal velocity invariant for all the frequency components contained in the broad spectrum of a short pulse. This generalization leads to a modification of the orbital angular momentum definition. Another generalization is introduced by considering helicoidal waves with a finite number of turns. We demonstrate that in this last case, the topological charge is no longer an integer. This provides a physical interpretation to vortices of fractional charge that are here involved to take into account the diffraction occurring at both tips of the now finite helical wavefront. We show that shortening the pulse implies an angular localization of the wave energy and as a consequence, a spreading of the angular momentum amplitude due to the uncertainty principle.

PACS numbers: 43.20.-f, 42.25.-p, 42.50.Tx

I. INTRODUCTION

This article presents a generalization of acoustical or optical vortices to the transient regime. We consider the case for which polarization can be neglected and hence deals with scalar wavefields only. The theory presented in a first part is then illustrated by experiments with ultrasound in water.

In a homogeneous medium, optical or acoustical fields are generally named according to the geometry of their wavefront, such as plane, cylindrical or spherical waves. There also exist waves whose wavefront is a helicoid. Hence, these ones are called spiral or helical waves, but also and more commonly either optical or acoustical vortices (as they are associated with an angular momentum) or sometimes screw dislocations. The similarity between the geometry of the wavefront and the atomic plane of a screw dislocation in crystallography [1] explains this last denomination. Optical vortices carry a finite orbital angular momentum of $l\hbar$ per photon [2], where l is an integer called the topological charge. It is this charge, or orbital angular momentum, which confers to these special waves many interesting properties for transport of information [3], [4], [5], remote control of objects [6], ... This field of research is growing fast and a lot of works have been published in optics in the past few years. The properties of optical and acoustical vortices in fluids are closely related for paraxial waves, [7], [8]. However, contrarily to optics, the speed of sound is non dispersive for most of the media, so that the nonlinear interaction is more efficient in acoustics, high order harmonics being easily obtained (this is the so-called "harmonic cascade"). Recently, the regime of weak helical acoustical shock waves has been investigated first numerically [9] and then experimentally [10]. Parametric antennas can also been used to carry out nonlinear combinations of several states and so perform basic arithmetical computations using the topological charge [11]. Furthermore, the finite angular momentum carried by an acoustical vortex can be transfered to matter [12].

In all these studies, the waves are either monochromatic or quasi-monochromatic: a wave train of at least a dozen of cycles. In optics, an intensive field of research is developing for ultrashort femtosecond pulses [13], [14]. However even if the laser pulses have a duration of about 6 fs and hence 2 cycles, the latest results show that the shortest pulses obtained for optical vortices are wave packets of about 25 fs of duration and hence, contain about 10 cycles [15], [16], which is quite comparable to experiments performed in acoustics [8]. These works, with coherent femto-second sources, were preceded by studies on white-light vortices (see [17] and references therein), for which the spectrum is in the range 475-600 nm, and hence has a relative bandwidth of 25% comparable to vortices obtained with femto-second sources [15], [16]. Even if the bandwidth may be much larger by non linear steepening, [10], the wave is still made of the superposition of wave trains of a dozen of cycles at each harmonic. In all these cases the topological charge is an integer proportional to the order of the harmonics, [8].

The usual modeling of a monochromatic vortex for a scalar wave field in cylindrical coordinates (r, θ, z) is then:

$$\psi(r, \theta, z, t) = F(r, z, \omega) \exp\{i(l\theta + k\varphi(r, z) - \omega t)\}, \quad l \in \mathbb{Z} \tag{1}$$

with l the topological charge, $k = \omega/c$ the wavenumber, ω the angular frequency, c the phase velocity, z the main axis of propagation of the wave and $\varphi(r, z)$ the phase dependency on the radial (r) and axial (z) coordinates. The radial dependence is less important and many formulations exist. The most popular are Laguerre-Gaussian (LG), r-vortex (RV), and Bessel waves see, Tab. I.

Model	$F(r, z, \omega)$	$\varphi(r, z)$
LG	$\frac{A}{w(z)} \exp\left(\frac{-r^2}{w^2(z)}\right) \left[\frac{\sqrt{2}r}{w(z)}\right]^{\lvert l\rvert} L_p^{\lvert l\rvert}\left(2r^2/w(z)^2\right)$	$k^{-1}(2p + \lvert l\rvert + 1)\arctan(z/z_R) - \frac{r^2 z}{2\left(z^2+z_R^2\right)}$
RV	$Ar^{\lvert l\rvert} + Br^{-\lvert l\rvert}$	1
Bessel	$AJ_l(\kappa r)$	k_z/k

TABLE I. Different models for paraxial helicoidal waves

here $w(z) = w_0\sqrt{1 + z^2/z_R^2}$ is the beam width at z, w_0 is the beam waist, $z_R = \pi\omega^2/\lambda$ the Rayleigh range, λ the wavelength and $(2p + |l| + 1)\arctan(z/z_R)$ the Gouy phase. A and B are real constants. The number p is related to the number of nodes in the radial direction. κ is related to k_z by the dispersion relation $k^2 = k_z^2 + \kappa^2$ and determines the radial dependence. Laguerre-Gaussian modes are a complete set of solutions of the paraxial approximation of Helmholtz's equation, whereas Bessel waves, i.e. cylindrical waves, are a complete set of solutions of Helmholtz equation (plane waves can be expanded into cylindrical waves with the Jacobi-Anger relation).

The key properties of the vortex arise from the azimuthal angle dependence with a finite l, and distinguishes these waves from other non diffracting ones, like Bessel waves of order 0 [18], or X waves [19].

One can observe that the condition $l \in \mathbb{Z}$ is related to the continuity of the field with the polar angle θ. Indeed as

trigonometric functions are periodic of period 2π, one gets:

$$\lim_{\theta\to+\pi}\psi\left(r,\theta,z,t\right)=\lim_{\theta\to-\pi}\psi\left(r,\theta,z,t\right)\Leftrightarrow l\in\mathbb{Z}. \tag{2}$$

This condition is required since valid solutions of the homogeneous Helmholtz equation are differentiable. However, vortices of fractional charge, $l\in\mathbb{R}$, have been studied theoretically [20, 21], and observed experimentally [22]. However these waves do not propagate unaffected in free space, are not axisymmetric and can be written as a sum of integer vortices (or cylindrical waves of integer order) [20, 21]. Cylindrical waves of fractional order have also been called helical beams [23] and erroneously presented as a generalization of Bessel beams. Indeed in this last reference, the helical beam, Eq. 10, transformed from helical to cylindrical coordinates is equal to a Bessel beam, Eq. 8, but with a fractional order q. We will show that solutions with a close resemblance to vortices of fractional charge are required in the generalization presented in this article and how, diffraction smoothes the discontinuity at $\theta=\pm\pi$ and leads to a solution compatible with Helmholtz equation in free space.

In part II of this article, we show that the definition of the phase of a vortex given by Eq. 1 implies that a short pulse on such an helicoidal wavefront has a time shape that varies with the polar angle. However this problem can be solved by generalizing Eq. 1 to transient signals. As a consequence the topological charge has now to vary with the frequency, and hence, can no longer be an integer for all the Fourier components contained in the broad spectrum of the pulse. However the concept of transient vortex has to be discussed. Indeed, by definition, the wavefront of a vortex is a helicoidal surface with an infinite number of turns. Hence, a line parallel with the axis of propagation intersects the wave front periodically at each turn. This situation contrasts with spherical or plane waves, for which the local wave vector intersects the wave front at a single point. We will show the consequences of such a periodicity on the topological charge. This analysis does not depend on the kind of waves (optical, acoustical...) and is valid for any field that can be modeled by a scalar wave function.

In part III, an experiment for acoustical vortices at a 1 MHz frequency illustrates this generalization for various charges. This experiment is carried out in the acoustical weak shock wave regime. The nonlinear aspect is discussed elsewhere [10], and here the shock front is used primarily as a marker facilitating the identification of the wave front for a broadband signal.

II. TRANSIENT VORTICES, TRUNCATED HELICOIDAL WAVEFRONTS AND FRACTIONAL CHARGE

A. A pulse whose shape remains constant with the azimuthal angle

For a monochromatic vortex of charge l described by Eq. 1, the wave vector is defined by:

$$\vec{k}=k\vec{n}=\overrightarrow{\nabla}\left(l\theta+k\varphi(r,z)\right)=k\left(\varphi_{,r};\frac{l}{kr};\varphi_{,z}\right) \tag{3}$$

where $\varphi_{,z}$ (resp. $\varphi_{,r}$) is the partial derivative of the function φ in direction z (resp. r). The wave vector component in the azimuthal direction is independent on frequency, whereas in direction z, it is as usual proportional to the angular frequency. Assuming that $\vec{n}$ is the refractive index, then its radial and axial component are independent of ω whereas its azimuthal component n_θ is inversely proportional to the angular frequency. This is in contradiction with the fact that we consider here a simple homogeneous, isotropic and non dispersive medium. The modification required to keep a constant l/k, and hence n_θ, consists in defining a new charge α proportional to the frequency:

$$\alpha\left(\omega\right)=l\omega/\omega_0. \tag{4}$$

Here we can choose $l\in\mathbb{Z}$ without any loss of generality since $\omega_0\in\mathbb{R}$ and can be adjusted continuously. This notation allows us to recover a vortex of integer charge l for $\omega=\omega_0$. A convenient choice for ω_0 is the central angular frequency of the pulse spectrum.

Applying the modified charge, Eq. 4, to Eq. 1 yields:

$$\psi\left(r,\theta,z,t\right)=F\left(r,z,\omega\right)\exp\left(i\left(l\theta\omega/\omega_0+k\varphi(r,z)-\omega t\right)\right),\ l\in\mathbb{Z}, \tag{5}$$

For consistency, one can check that the phase factor $\exp\left(il\theta\omega/\omega_0\right)$ becomes after an inverse Fourier transform a convolution product by $\delta(t-l\theta/\omega_0)$, where δ is the Dirac distribution and $*$ is the convolution product. Therefore the pulse propagates along θ without deformation and a complete turn is achieved in a time interval of lT_0 where $\omega_0=2\pi/T_0$.

This modification of the charge seems to lead to fractional order vortices but as discussed in the introduction, fractional order vortices are not solution of the Helmholtz equation. However we will show in the experimental part that pulse vortices does exist. This dilemma is solved in the two next sections II B, II C.

B. Helicoidal wavefronts with an infinite number of turns

On the one hand, the modification, Eq. 4, seems to impose a non integer charge α and thus, vortices of fractional charge for corresponding frequency components. On the other hand, the discussion below Eq.2 states that fractional order vortices are not valid solution of the wave equation in free space. Now, we will show that, when the number of turns of the helix is infinite, the spectrum is composed only of the spectral lines (the frequencies) for which the charge is an integer. This property is true whatever the shape of the pressure pulse. Indeed, let's choose a monochromatic function with an axisymmetric intensity and a charge fractional charge $\alpha = \omega l/\omega_0$:

$$\psi\left(r,\theta,z,t\right) = V\left(r,z,\omega\right)\exp\left(i\omega\left(\theta l/\omega_0 - t\right)\right), \tag{6}$$

By inverse Fourier transform of Eq. 6, one obtains the transient helicoidal beam:

$$v\left(r,z,t\right) * \delta\left(t - \frac{l\theta}{\omega_0}\right) = v\left(r,z,t - \frac{l\theta}{\omega_0}\right), \tag{7}$$

where v being the time representation of V. Clearly, Eq. 7 shows that the pressure pulse is simply retarded or advanced according to the sign of the charge. The time shift is linearly dependent on the polar angle with a slope equal to l/ω_0. Hence, the change applied on the definition of the topological charge, Eq. 4, ensures that the pulse now keeps its shape and is just time shifted. This time shift arises from the projection of the helicoidal wavefront onto the transverse plane. After one revolution in the transverse plane, or equivalently one turn of the helicoid, the time shift is equal to: $2\pi l/\omega_0 = lT_0$. The pitch of the helicoid is then, in a time representation (at fixed z), equal to lT_0. As noted before since $T_0 \in \mathbb{R}$, this pitch can be adjusted continuously. Up to now we have described only a single turn. In the monochromatic regime, the wavefront of a vortex is assumed to be a helicoid with an infinite number of periodic turns. This periodicity is a special feature of helicoidal beams compared to plane or spherical waves for instance. A display of a helicoidal surface with three turns and a pitch equal to one, compared to one turn and a pitch equal to three, is visible on Fig. 1. Each turn corresponds to a revolution of the pulse $\theta \to \theta + 2\pi$ in the transverse plane. To get an infinite number of turns, the simplest modification of Eq. 7 is to reproduce the pulse after

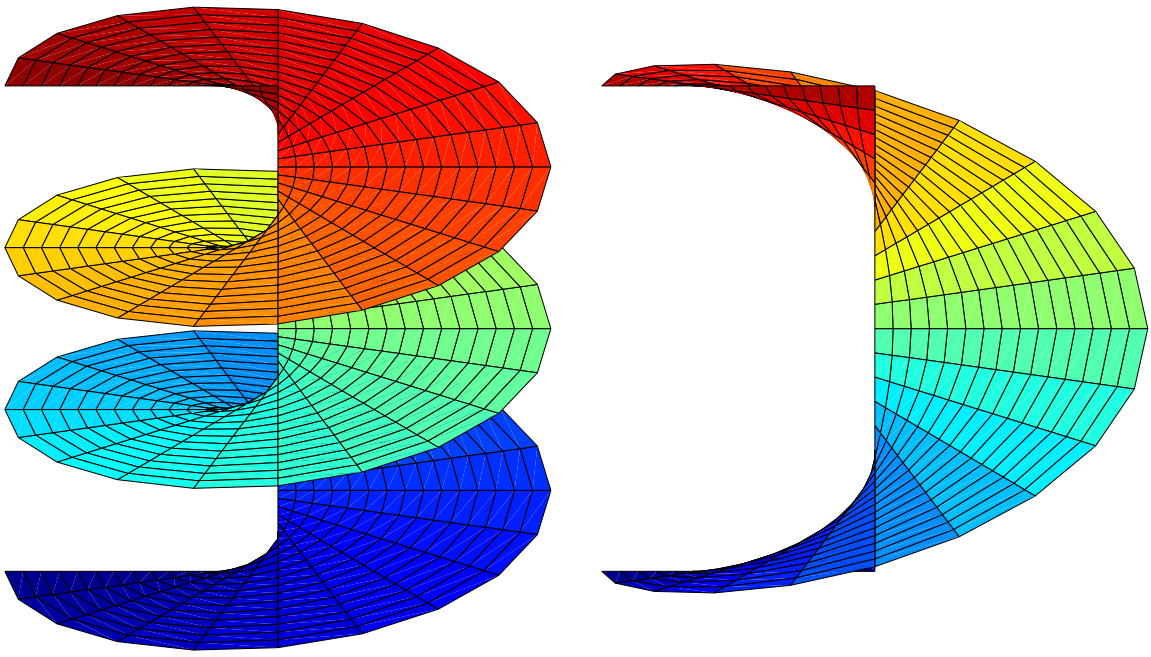

FIG. 1. (Color online) Helicoidal surface of pitch equal to 1 and truncated after 3 turns (left side), and of pitch equal to 3 truncated after 1 turn (right side)

each revolution, and hence with the period lT_0. Note that this corresponds to a helicoid with a 1-fold symmetry. To iterate the revolution of the pulse around the axis, it is convolved with a Dirac comb of period lT_0 to get:

$$v^p\left(r,z,t - \frac{l\theta}{\omega_0}\right) = v\left(r,z,t - \frac{l\theta}{\omega_0}\right) * \sum_{m=-\infty}^{\infty}\delta\left(t - mlT_0\right) \tag{8}$$

As the signal u^p is strictly periodic (as indicated by the superscript "p"), it can also be written as a Fourier series. Using the Fourier series of the Dirac comb:

$$\sum_{m=-\infty}^{\infty} \delta\left(t - mlT_0\right) = \sum_{m=-\infty}^{\infty} \exp\left\{im\omega_0 t/l\right\}, \tag{9}$$

and recognizing that thereafter, the convolution product is now a Fourier transform taken at discrete angular frequencies equal to $\omega = m\omega_0/l$, we get:

$$v^p\left(r, z, t - \frac{l\theta}{\omega_0}\right) = \sum_{m=-\infty}^{\infty} V\left(r, z, m\omega_0/l\right) \exp\left\{im\left(\theta - \frac{\omega_0}{l}t\right)\right\}. \tag{10}$$

This shows that the dilemma is a paradox when the pulse vortex is not truncated along its axis and hence is made of an infinite number of pulse. A pulse helicoidal beam is made of the superposition of monochromatic helicoidal beams at angular frequencies $\omega = m\omega_0/l$. These spectral lines are located at those frequencies for which the generalized topological charge, $\alpha = l\omega/\omega_0 = m \in \mathbb{Z}$, is an integer. This is the first important result of this work. This special feature comes from the helicoid pitch and the 1-fold symmetry considered for the wave front. These geometrical characteristics of the helicoidal wavefront introduce a time/space periodicity that does not exist for plane or spherical waves. This periodicity implies resonances in a transverse plane that can be compared to orbital resonances. Note that the helix pitch lT_0 is continuously adjustable for a pulse vortex as long as the pulse duration is shorter than the helix pitch. For longer pulses, constructive and destructive interferences between consecutive turns appear. For monochromatic wave of period T, the helix pitch is fixed by these interferences and equal to lT.

C. Fractional topological charges and truncated helicoidal wavefronts

Up to now we have considered an infinite number of turns for the helicoidal wavefront. Obviously, in practical situations, the number of iterations of the pulse, i.e. the number of turns of the helicoid, is finite. In this last case, the previous derivation is no longer valid. The helicoidal wave has now a finite number of turns and this limitation can be modeled by introducing a time window $w\left(t\right)$ to get a finite number of pulses, so that Eq. 8 now becomes:

$$v^w\left(r, z, t - \frac{l\theta}{\omega_0}\right) = v\left(r, z, t - \frac{l\theta}{\omega_0}\right) * \left[w\left(t\right) \sum_{m=-\infty}^{\infty} \delta\left(t - mlT_0\right)\right] \tag{11}$$

where the superscript w is introduced to distinguish the time windowed case from the periodic one. As the function v^w is no longer periodic, its Fourier series can not be used as previously. However Fourier series are just a special case of continuous Fourier transforms in the context of tempered distributions employed with square integrable test functions like the pulse v. Indeed the Fourier series in Eq. 10 is the inverse Fourier transform of the frequency domain representation of the periodic function v^p. So, the generalization of Eq. 10 consists in performing the Fourier transform of Eq. 11 to get the field representation at a given angular frequency ω:

$$\psi^w\left(r, z, \theta, z, t\right) = V\left(r, z, \omega\right) \exp\left\{i\omega\left(\frac{l\theta}{\omega_0}\right)\right\} \left[W\left(\omega\right) * \sum_{m=-\infty}^{\infty} \delta\left(\omega - \frac{m}{l}\omega_0\right)\right] \exp\left\{-i\omega t\right\} \tag{12}$$

To get the above equation, on the one hand, products are replaced by convolution products and vice versa. On the other hand, the identity between a Dirac comb and its Fourier series, Eq. 9 applied now to the Dirac comb of Eq. 11 is used as usual to show that the Fourier transform of a Dirac comb of period lT_0 is a Dirac comb of period ω_0/l.

When comparing the finite helicoidal case Eq. 12 to the infinite and hence periodic one Eq. 10, one sees that the energy remains distributed on spectral lines $\omega = ml/\omega_0$, but these lines are now no longer infinitely narrow: their width depends on the spectrum of the window, $W(\omega)$, or equivalently, on the duration of the time window $w(t)$, i.e. on the number of turns of the helicoidal wavefront. The shorter the signal (i.e. the less the number of turns of the wavefront), and the larger the relative importance of the components with a non integer charge will be. Note the field can be made up of an arbitrary number of turns, and even of a fraction of a single turn. A single turn is a special case. In that case, as the pulse repetition does no longer take place, the field fully looses its time/axial periodicity, the spectral lines associated with that periodicity disappear and the signal spectrum is simply the source pulse spectrum $V(r, \omega)$.

Therefore, the dilemma is more complex when the number of pulse is finite. The truncation widens the spectral lines and at these new frequencies, the present analysis leads to fractional order Bessel beams. A fractional charge leads to a discontinuity, Eq. 2, supposed to be located at $\theta = \pm\pi$ here. The polar angle ranges in the interval $\theta \in [-\pi, +\pi[$ only, and hence, the field is not multi-valued. However, such a discontinuous function is not a solution of the homogeneous Helmholtz equation in free space. $\exp(i\alpha\theta)$ is a periodic function of θ and can be approximated by a Fourier series involving integer vortices only, see the appendix. This series is truncated to fit in the angular spectrum bandwidth of the wave ensuring that the solution is two times differentiable. Therefore the actual solution has a close resemblance with a vortex of fractional order. It consists in keeping a phase proportional to θ everywhere but over an angular sector around the discontinuity where the evolution is no longer linear in order to connect the two parts continuously. This behavior will be confirmed in the experimental part, Fig. 10, and the appendix provides a derivation of the existence of diffraction and the loss of the circular symmetry. Indeed, monochromatic vortices with a single integer charge (like a sum of Bessel waves of different κ but identical l) may diffract radially but their azimuthal dependence does not depend on the distance of propagation. Hence the field keeps its circular symmetry for the intensity. However, the truncation of the number of turn of the helicoid breaks this circular symmetry. The existence of beginning and end tips of the wave front implies diffraction along θ. That diffracting part requires superposition of vortices of different charges at the angular frequency considered. This is the signification of the spectral lines widening.

This section concludes the generalization to transient regime of helicoidal beams. Two characteristic times were identified in the previous section: the pulse duration and the helix pitch lT_0. A third is defined by the truncation of the wavefront: the number of pulses times the helix pitch. This last characteristic time breaks the helical symmetry and induces azimuthal diffraction. The dilemma is hence a paradox and pulse helicoidal wave with finite or infinite wavefronts have been described.

D. The geometry of the wavefront

A remark can be made about the geometry of the wavefront. Let's introduce the variable s, which is identical to the polar angle θ over the range $[-\pi, \pi[$ but without the 2π periodicity:

$$s = \theta + 2\pi\ m,\ m \in \mathbb{Z}. \tag{13}$$

If we consider a r_vortex [1] for which $F(r) = r^{\pm\alpha}$, and, $\varphi(r, z) = z$ then the equiphase surface is defined by the condition, Eq. 8:

$$-\frac{ls}{\omega_0} = \frac{z}{c}. \tag{14}$$

Using s to parameterize the surface yields:

$$\begin{cases} x = r\ \cos(s) \\ y = r\ \sin(s) \\ z = -\dfrac{lcs}{\omega_0}. \end{cases} \tag{15}$$

This is the definition of a 1-fold symmetrical half helicoid of pitch $lcT_0 = l\lambda_0$ and a drawing of this surface is displayed on Fig. 1. Indeed, a helicoidal surface is a ruled surface, that may be constructed by moving a straight line (by a rotation in the transverse plane (x, y) along with a translation along the axis). A fully infinite line will give rise to a double helix, while a single helix is obtained by a semi-infinite half line ($r \geq 0$). The vortex wave fronts considered here are only single helices. The 1-fold symmetry means that i) the wave front is periodic and ii) the period is a single turn around the axis. Thus the helix pitch in space representation (at fixed t), is $clT_0 = l\lambda_0$ and, in time representation (at fixed z), is lT_0.

E. The orbital angular momentum

This modification of the topological charge from an integer l to a real $\alpha = l\omega/\omega_0$, Eq. 4, induces a change of the orbital angular momentum expression. First we consider monochromatic vortices of fractional charge and then we take into account the fact that an pulse vortex is the superposition of vortices of different angular frequencies.

Considering paraxial and monochromatic waves only, and following the derivation of [2], yields an analog expression for the orbital angular momentum scalar component along z, $\mathcal{M}_z$, but where l is replaced by $\alpha = l\omega/\omega_0$. In the

following, $\psi(r,\theta,z,t)$ is either the potential vector of a linearly polarized optical wave, $\vec{A}=\psi\vec{x}$ [2], or the scalar potential vector of a longitudinal acoustical wave [7], [8]. In both case, the momentum density, $\vec{\mathcal{G}}$, is equal to the Poynting vector, $\vec{\mathcal{P}}$, divided by c^2 and written per unit power gives:

$$\vec{\mathcal{G}}=\frac{\vec{\mathcal{P}}}{c^2}=-\frac{i\omega\epsilon}{2}\left(\phi^*\vec{\nabla}\phi-\phi\vec{\nabla}\phi^*\right), \tag{16}$$

in which $\psi(r,\theta,z,\omega)=\phi(r,\theta,z,\omega)\exp(-i\omega t)$, ϵ is the permittivity of the medium in optics, and $\epsilon=\rho_0/c^2$ is the ratio between the density and the square of the phase velocity in acoustics. Note we use here ϵ as in [8] and not ϵ_0 as in [2], so that $\vec{\mathcal{G}}$ is indeed the pseudo momentum. The orbital angular momentum density per unit power is:

$$\vec{\mathcal{M}}(r,z,\theta,\omega)=\vec{r}\wedge\vec{\mathcal{G}}(r,z,\theta,\omega). \tag{17}$$

In cylindrical coordinates, its component along z is:

$$\mathcal{M}_z(r,z,\theta,\omega)=-\frac{i\omega\epsilon}{2}\left(\phi^*\phi_{,\theta}-\phi\phi^*_{,\theta}\right). \tag{18}$$

The potential field, ψ is written as in Eq. 1 but now the topological charge is a real, α, defined in Eq. 4:

$$\psi(r,\theta,z,\omega)=\phi(r,\theta,z,\omega)\exp(-i\omega t)\,;\,\phi(r,\theta,z,\omega)=V(r,z,\omega)\exp(i\alpha\theta) \tag{19}$$

yields:

$$\mathcal{M}_z(r,z,\theta,\omega)=\epsilon\omega\alpha|\phi|^2 \tag{20}$$

Compared to the expression derived for monochromatic fields of integer charge, the modification of the charge leads to an orbital angular momentum that is no longer proportional to the frequency, but has the same quadratic dependency as the energy :

$$\mathcal{E}=\omega^2\epsilon|\psi|^2 \tag{21}$$

Here we have assumed that for a paraxial wave the kinetic and potential densities of energy (acoustics) or the electric and magnetic densities of energy (optics) are equal. For each frequency component, the ratio of Eqs. 20 and 21 gives a constant:

$$\frac{\mathcal{M}_z(\omega)}{\mathcal{E}(\omega)}=\frac{l}{\omega_0} \tag{22}$$

This relation is different of the one derived in [2] since the denominator is ω_0 and not ω. This ratio l/ω_0 depends on the helix pitch only. That result is reminiscent of the relation derived for energy pumping on the harmonics in the non linear regime [24], [8], and signifies that the wavefront has the same geometry for all frequencies. This relation is generalized here to all the frequency components, either belonging to the pulse bandwidth at the source, or arising from nonlinear transfers between harmonics during propagation. For isotropic and non dispersive media, the wave vector is perpendicular to the wave front. Thus Eq. 22 implies that the wave vectors are all aligned. This means that the phase-matching condition of wave vectors addition for non linear harmonics generation is satisfied. The condition of addition of angular frequencies is also satisfied for a non dispersive medium. Hence in non linear regime, the pulse will keep its shape but, for the non linear steepening coming from harmonics generation, that may lead to shock formation.

When the helicoidal wavefront has an infinite number of turns, this generalization to short pulses leads to quantized angular frequencies $\omega=m\omega_0/l$, Eq. 10. In that case, the pulse vortex is the superposition of monochromatic vortices of integer charge m. Since there is a single charge at each frequency the circular symmetry is maintained. These monochromatic vortices have different charges and hence are orthogonal modes when the integration on θ is carried out:

$$\frac{1}{2\pi}\int_{-\pi}^{+\pi}\exp\left(i\left(m_1-m_2\right)\theta\right)d\theta=\delta^{m_2}_{m_1}. \tag{23}$$

Therefore, the orbital momentum of short pulses on an infinite helicoidal wavefront is the sum of the orbital momentum of the integer charge vortices at angular frequencies $\omega=m\omega_0/l$ and charge m. This is a generalization of the result obtained in [2].

When the helicoidal wavefront has a finite number of turns, angular frequencies are no longer quantized. Moreover, as is demonstrated in the appendix and discussed previously the azimuthal component of the Poynting vector and hence $\mathcal{M}_z$ are now varying with θ, this last quantity is no longer axisymmetric. This behavior is due to the diffraction localized at the angle where the field would be discontinuous. Let's note:

$$\phi\left(r,\theta,z,\omega\right)=V\left(r,\theta,z,\omega\right)\exp\left\{i\varphi\left(r,\theta,z,\omega\right)\right\} \tag{24}$$

Compared to Eq. 19, this takes into account fields that are not axisymmetric. If we compute the integral of the ratio, $\mathcal{M}_z/\mathcal{E}$ along a closed curve around the singularity at r fixed, we get:

$$\langle\frac{\mathcal{M}_z}{\mathcal{E}}\rangle_\theta=\frac{1}{2\pi}\int_{-\pi}^{+\pi}\frac{\mathcal{M}_z}{\mathcal{E}}d\theta=\frac{1}{2\pi}\frac{1}{\omega}\Im[\int_{-\pi}^{+\pi}\frac{\phi_{,\theta}}{\phi}d\theta]=\frac{1}{2\pi}\frac{1}{\omega}\Im[\int_{-\pi}^{+\pi}\left(i\varphi_{,\theta}+\frac{V_{,\theta}}{V}\right)d\theta] \tag{25}$$

where $\Im$ is the imaginary part. If we consider free space far enough from any sources, we have continuity of the field :

$$\forall\theta,\ \phi\left(r,\theta,z,\omega\right)=\phi\left(r,\theta+2\pi,z,\omega\right) \tag{26}$$

So that, Eq. 25 yields:

$$\langle\frac{\mathcal{M}_z}{\mathcal{E}}\rangle_\theta=\frac{1}{2\pi\omega}\left(\varphi\left(r,+\pi,z,\omega\right)-\varphi\left(r,-\pi,z,\omega\right)\right)=\frac{n}{\omega} \tag{27}$$

with $n\in\mathbb{Z}$. Therefore this quantity multiplied by ω is quantized at each frequency even for truncated helicoidal waves. If the energy is $\hbar\omega$ per particle like for optical vortices then we recover an orbital momentum of n per photon. This is the last important result of this paper and complete the generalization of helicoidal beams to transient regime. However the ratio of the integrals is not quantized:

$$\frac{\langle\int_0^\infty\mathcal{M}_z rdr\rangle_\theta}{\langle\int_0^\infty\mathcal{E}rdr\rangle_\theta} \tag{28}$$

An analytical expression can be derived in some particular cases [22], [21]: $p-\sin\left(2\pi p\right)/2\pi$, and this behavior has been experimentally confirmed in [22].

III. ULTRASONIC EXPERIMENTS

A. Experimental set-up

The experimental set-up, Fig. 2 and the inverse filtering technique used to synthesize complex wave field pattern in linear and nonlinear acoustics have been described previously [25], [10]. The distance between the array and the control plane is $z=450\ mm$, where $z=0$ is the location of the source. The main difference here is in the choice of the pressure pattern $U(r,\omega)=F(r)E(\omega)$ that we use as an input for the inverse filtering technique. The radial dependence $F(r)$ of the pressure field is a Bessel function or order l multiplied by a Kaiser-Bessel window. The radial dependence is identical for all frequency components. The Kaiser-Bessel window is used to limit the lateral extension of the field and provide a solution compatible with the limited aperture of the array. The time dependence of the signal is adjusted to the bandwidth of the array of transducers, the acoustic source. This stage is carried out by defining its spectrum $E(\omega)$ as a Kaiser-Bessel window centered on the central angular frequency $\omega_0/2\pi=1.1$ MHz (corresponding to a wavelength close to 1.5 mm in water) and whose width is equal to the bandwidth of the transducers. This spectrum is multiplied by i to get a pure imaginary function in the Fourier representation, and hence an odd function in time. An odd function allows to get a shock at the middle of the pulse after non linear propagation. This procedure is used to get a pulse as short as possible and close to the duration of a single cycle at half amplitude, see Fig. 4.

To check the feasibility of these helicoidal beams, we synthesize transient vortices of pitch $3T_0$ and $4T_0$ so that the charge will be 3 and 4 at $\omega=\omega_0$ respectively. Each of these beams are synthesized for either 1, 2 or 10 helix turns, Fig. 3. The selection of the number of turns is achieved by varying the duration of the time window $w(t)$, chosen as a square window of respectively 1, 2 or 10 times the pitch. The signal to apply at the boundary condition (the array at $z=0$) to recover the "target" signal Eq. 12 at $z=450mm$, is determined by inverse filtering [8]. The pressure field, $p(x,y,z,t)$, is then measured on a square $(x,y)\in[-20\ mm,+20\ mm]$ perpendicular to the beam axis z and centered on it. The scanning step is $\Delta x=\Delta y=0.5\ mm$ in both directions. These measurements are made either at $z=450\ mm$ or $z=600\ mm$ away from the array.

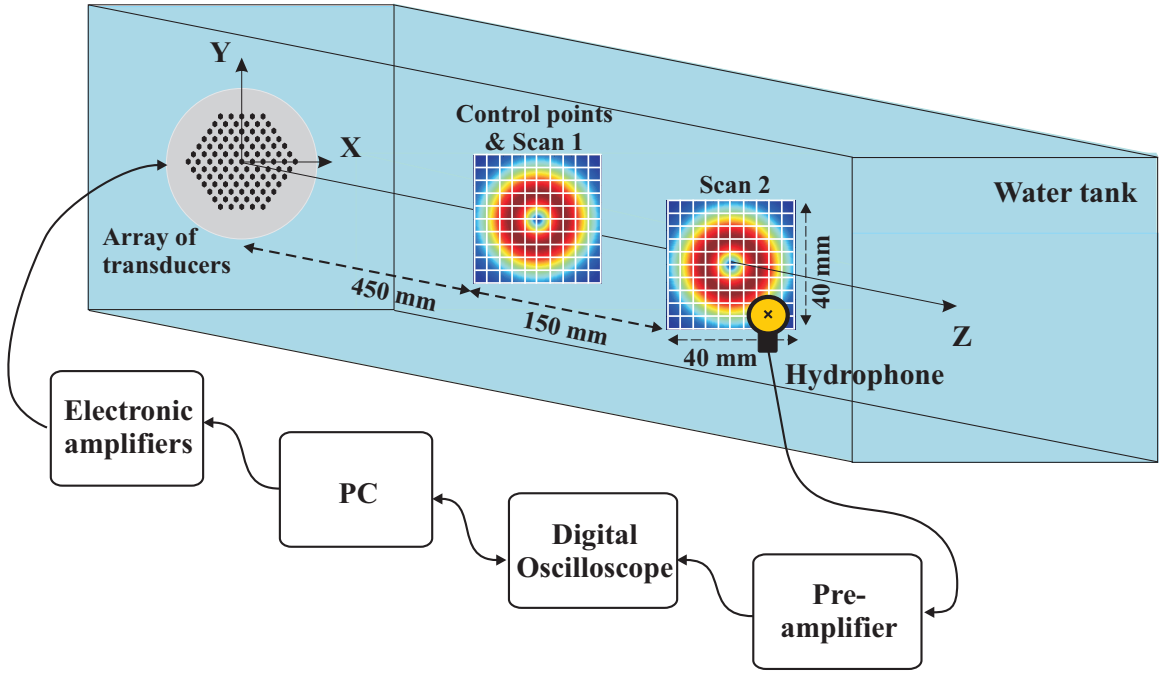

FIG. 2. (Color online) Sketch of the experimental set-up. The measurements are made at $z = 450\ mm$ and $z = 600\ mm$ whereas the fields is synthesized by inverse filtering at $z = 450\ mm$

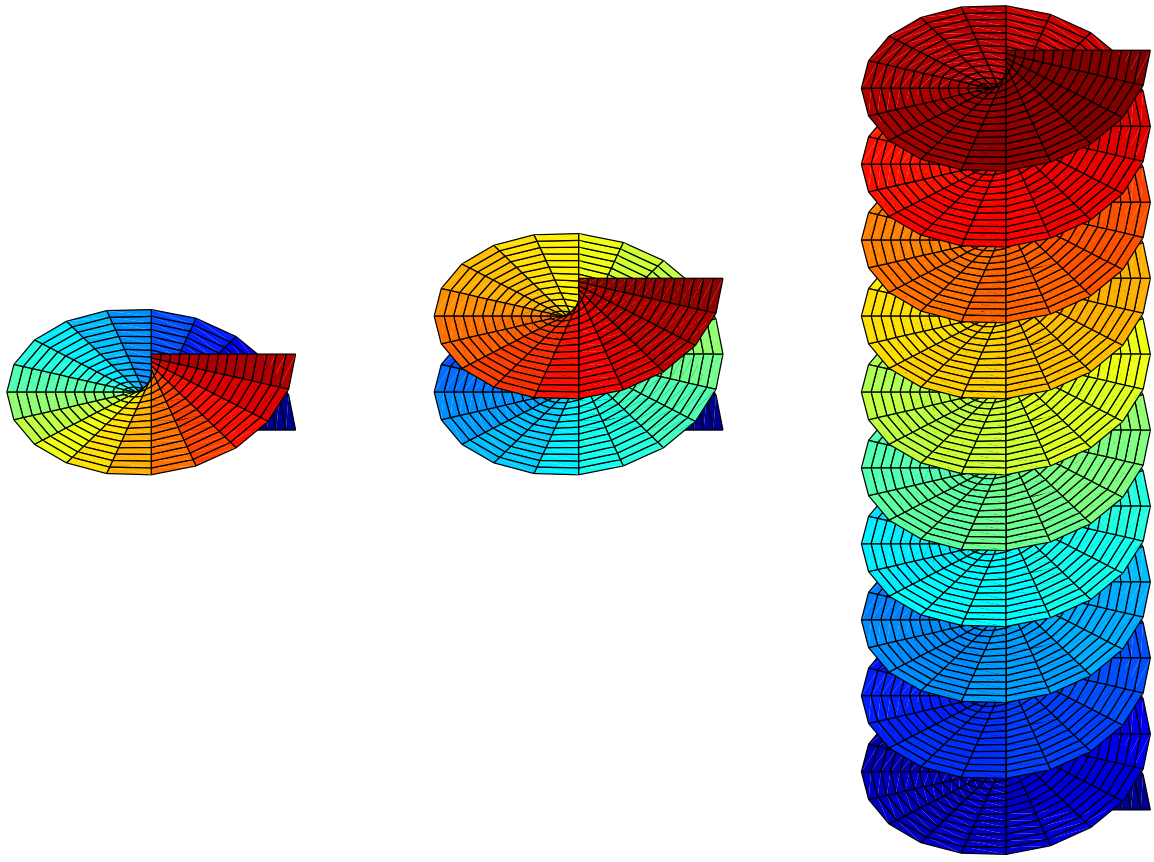

FIG. 3. (Color online) Wavefront for a helicoidal beam with 1 turn (left), 2 turns (middle), and 10 turns (right).

B. Spectrum of a pulse vortex beam - integer and fractional charges

The time waveforms and frequency pressure spectra (modulus of the Fourier transform of the time waveforms) measured at one point localized on the vortex ring at $z = 600\ mm$ are presented on Fig. 4 . As expected from Eq.

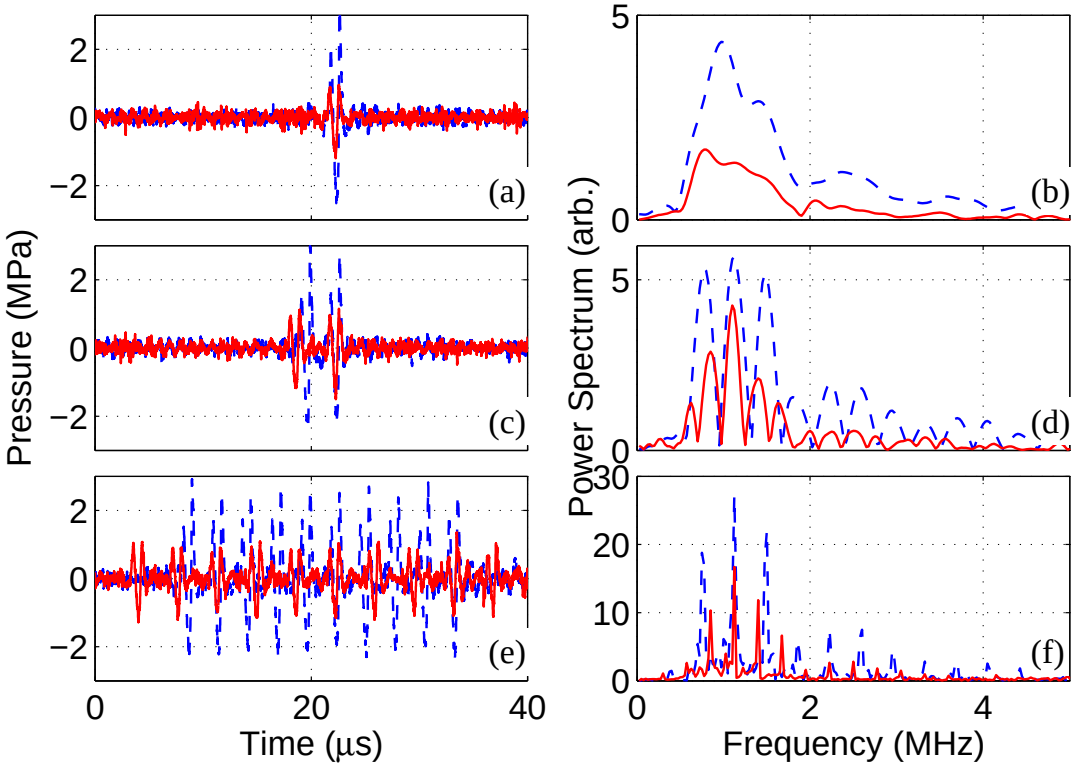

FIG. 4. (Color online) Pressure time signal ((a), (c), (e)) and frequency spectrum ((b), (d), (f)) measured at $z = 450mm$ for transient vortices of pitch 3 T_0 (blue dashed curves) and 4 T_0 (solid red curves) and for 1 ((a), (b)), 2 ((c), (d)) and 10 ((e), (f)) helix turns.

12, the energy is distributed on spectral lines whose width is determined by the width of the window $W(\omega)$. Indeed, for long signals (10 turns, (e) and (f) subplots), the spectral lines are very sharp and narrow with little energy in between, while, when the width of the window $w(t)$ is reduced to 2 turns ((c) and (d) subplots), the spectral lines, while still visible, overlap and enlarge to fill the whole spectrum. For both cases, the time lag, lT_0 see above, between two consecutive pulses is equal to the pitch, and hence, the orbital resonances are closer when l increases (from dashed to solid lines (resp. blue to red online)). For the shortest window, only one turn remains ((a) and (b) subplots), the spatial periodicity of the helix is fully lost and modulation in the frequency domain disappears. In this last case, the observed spectrum is simply the one of the elementary pulse $E(\omega)$. In summary, the position of the spectral lines depends on the helix pitch. They correspond to frequencies for which the topological charge is an integer, whereas the line-width is related to the number of turns. The energy located between the spectral lines increases when the number of turns decreases. This increasing importance is correlated with the relatively enhanced diffraction occurring at the tips of the finite helicoidal wavefront. At the head and tail of the wavefront the beam intensity is no longer axisymmetric. Modeling such a beam requires a sum of integer order vortices. We will see below that this summation results in a continuous field that has a close resemblance with a fractional order vortex. Note also that the number of spectral lines depends on the bandwidth of the pulse. In the linear regime, they should be confined within the bandwidth of the transducers, here 0.6-1.6 MHz. However since the propagation is here non linear, the bandwidth of the elementary pulse, 0.6-1.6 MHz, is duplicated by nonlinear harmonic pumping so that the frequency spectrum extends up to 4 MHz.

C. Short pulses and large number of turns

In this section, we are interested in vortices with a large or infinite number of turns. In this case the field is periodic with a period equal to the vortex pitch lT_0. From the pressure amplitude, $p(r, \theta, z = 600, t)$ measured on a transverse plane at $z = 600\ mm$, the data corresponding to a ring of width 0.5 mm and radius $12mm$ ($r \in [12, 12.5]$) for the vortex of pitch $3T_0$ and $r \in [15, 15.5]$ for the vortex of pitch $4T_0$ are extracted and displayed on Fig. 5. Here we plot the pressure amplitude in gray scale and in unit of MPa (color online) for a window of duration one period lT_0 located in the middle of the wave train, visible on Fig. 4, subplot (e). This behavior is hence characteristic of pulse vortices with an infinite number of turns. The pressure amplitude is about 0.5 MPa so that at $z = 600\ mm$ a shock wave is obtained. This explains the fast transition of the pressure field from negative to positive values and is used to facilitate the identification of the wave front. The pulse is time shifted proportionally to the polar angle and a turn is carried out in lT_0. One can also check that the pulse shape is constant in both cases even if weak amplitude modulation is present, i.e. the azimuthal dependence is a phase term proportional to the frequency. This is a first confirmation of the validity of the modification of the charge Eq. 4 and 8.

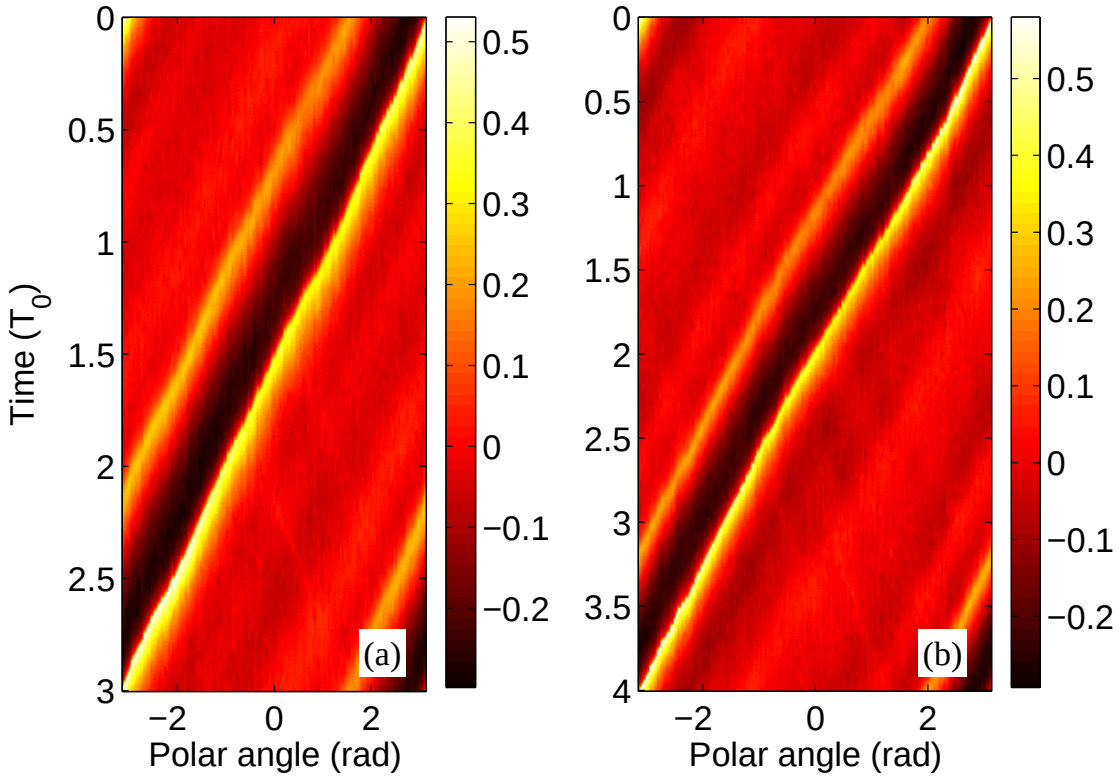

FIG. 5. (Color online) Pressure amplitude (gray scale in MPa) measured at $z = 600mm$ for transient vortices of pitch 3 T_0 (subplot (a)) and 4 T_0 (subplot (b)) on a ring of width $0.5mm$ and radius $12mm$ and $15mm$ respectively. The vortices are made of 10 turns, but one located in the middle is presented

(subplot (a))

From the instantaneous pressure amplitude, $p(x, y, z = 600, t)$, measured on the whole transverse plane $(x, y) \in [-20\ mm, +20\ mm]$, a Fourier transform is performed to get : $p(x, y, z, \omega)$. The modulus is displayed on subplots (a), (b) and (c) for 3 frequencies ($\omega/\omega_0 = 2/3,\ 1$ and $4/3$), Fig. 6. The phase is computed using the usual formula $\arg(p) = \arctan\left(\Im(p(r, \theta, z, \omega))/\Re(p(r, \theta, z, \omega))\right)$ where $\Re$ is the real part. This result in a phase folded in the interval $[-\pi, +\pi]$. This phase is displayed in gray (color online) scale for 3 same frequencies subplots (c), (d) and (e). These 3 frequencies correspond to the center of the three main spectral lines in the case of a window $w(t)$ of duration 10 turns, Fig. 4 (subplot (f)). The phase increases clockwise from $-pi$ to $+pi$ and the number of 2π steps after a complete turn is the topological charge. This demonstrates that these beams carry an integer topological charge (respectively

α = 2, 3 and 4), increasing by one unity from one line to the next one, in agreement with the generalized charge of Eq. 4. Note that the intensity ring is closed and almost axisymmetrical, so that the charge is indeed an integer.

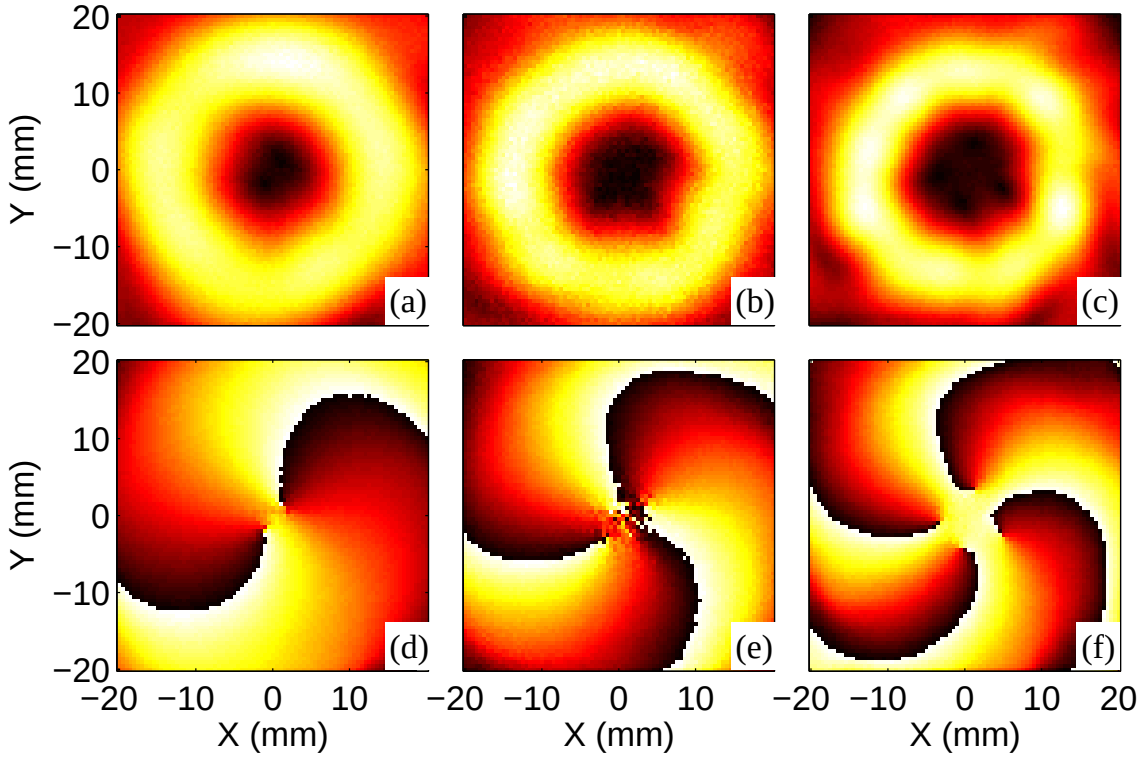

FIG. 6. (Color online) Modulus arb. unit (subplot (a), (b) and (c)) and phase $[-\pi, +\pi]$ (subplot (d), (e) and (f)) in gray scale. This subplot corresponds to the vortex of pitch 3 T_0, duration 10 turns and measured at $z = 600mm$. 3 angular frequencies located on the three main spectral lines of Fig. 4: $2/3\omega_0$ (subplot (a) and (d)), $3/3\omega_0$ (subplot (b) and (e)) and $4/3\omega_0$ (subplot (c) and (f)) are selected

.

To confirm further that the charge is an integer, the phase dependence with the angle θ on a large radius of 12 mm and 15 mm respectively for vortices of pitch $3T_0$ and $4T_0$ is extracted and displayed on Fig. 7 (a) and (b). The phase displayed on Fig. 6 is folded in the interval $[-\pi, +\pi]$. The 2π step are then unwrapped with a classic algorithm and a continuous curve is recovered. The width of the rings is as before 0.5 mm. The three frequencies selected for the vortex of pitch $lT_0 = 3T_0$ (left figure) and $lT_0 = 4T_0$ (right figure) are $\omega_0(l-1)/l$ (solid blue line), ω_0 (dashed red line) and $\omega_0(l+1)/l$ (dashed-dotted green line). These frequencies correspond to the three spectral lines of highest amplitudes, Fig. 4. The phase for $\theta = -\pi$ has been subtracted so that the three curves start at the origin of the graph. These three figures are computed for the three spectral lines of both vortices on the same large ring mentioned before. The phase is obviously linear with the polar angle. The slope computed with a linear regression is given in Tab. II. The fitting straight lines are plotted on the same figure so that the goodness of fit can be easily assessed. These figures confirm that the charge is an integer, the phase is proportional to the azimuthal angle, the charge increases from one unity from a spectral line to the next one since it is proportional to the frequency, Eq. 4.

To compute the charge, different methods can be proposed : the phase slope, the phase increment when θ varies of 2π, Eq. 27, and from the average of the orbital momentum normalized by the energy, Eq. 25. All these methods are equivalent, Tab. II, if the theoretical analysis developed previously is valid and can be applied to this experiment. Since the phase can be calculated without any derivative, the signal to noise ratio is better for the first two techniques.

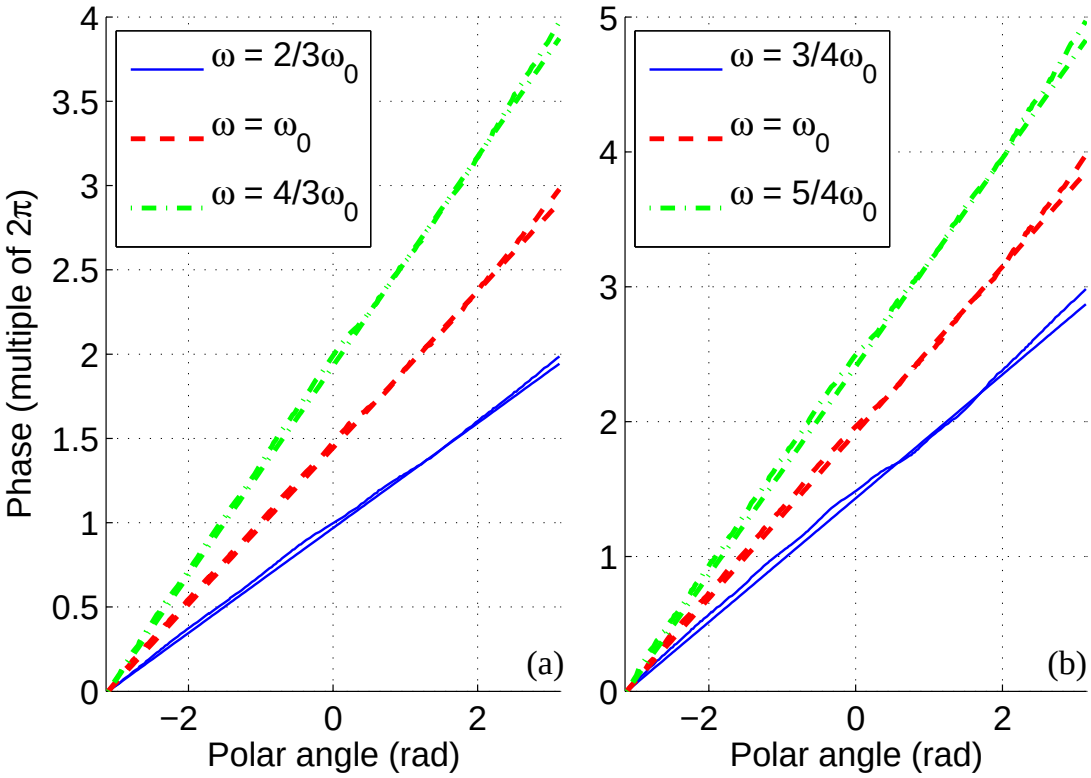

FIG. 7. (Color online) Phase measured at $z = 600mm$ for transient vortices of pitch 3 T_0 (a) and 4 T_0 (b) on a ring of width $0.5mm$ and radius $12mm$ (a) and $15mm$ (b) respectively. 3 angular frequencies located on the three main spectral lines of Fig. 4: $(l-1)/l\omega_0$ (solid blue line), ω_0 (dashed red line) and $(l+1)/l\omega_0$ (dashed-dotted green line).

Vortex pitch $3T_0$ $r \in [12, 12.5]mm$				Vortex pitch $4T_0$ $r \in [15, 15.5]mm$			
ω	Phase/2π slope	$\omega\times$Eq. 25	$\omega\times$Eq. 27	ω	Phase/2π slope	$\omega\times$Eq. 25	$\omega\times$Eq. 27
$2/3\omega_0$	2.0	2.0	2.0	$3/4\omega_0$	2.9	2.9	3.0
ω_0	2.9	3.0	3.0	ω_0	3.9	3.8	4.0
$4/3\omega_0$	3.9	4.0	4.0	$5/4\omega_0$	4.9	4.8	5.0

TABLE II. Phase slope in multiple of 2π and average of local density of angular momentum multiplied by ω on a ring of large radius. This ring is located where the pressure amplitude takes its highest values.

D. Short pulses and a finite number of turns

The same analysis is performed for the same vortices but now the helicoid is truncated after one turn, Fig. 4 subplots (a) and (b). As in the previous section, the pressure amplitude, measured on a ring of width 0.5 mm and radius 12 mm for the vortex of pitch $3T_0$ (subplot (a)) and 15 mm for the vortex of pitch $4T_0$ (subplot (b)), is displayed on Fig. 8. However here the whole signal is presented and the time window is $(l+1)T_0$ where $l = 3$ or 4. Again the pulse shape is invariant and time shifted proportionally to the polar angle for location far from the edges of the wavefront located here at $\theta = -2$. The difference with the infinite helicoids is the diffraction at the beginning and the end of the truncated helicoidal wavefront where the shape is varying (the phase slope is no longer proportional to the frequency) here around $\theta = -2$ rad. Angular frequencies $\omega/\omega_0 = 2.25/3$, $2.5/3$ and $2.75/3$, expected to correspond respectively to charge $\alpha = 2.25$ (subplots (a) modulus and (d) phase), 2.5 (subplots (b) modulus and (e) phase) and 2.75 (subplots (c) modulus and (f) phase), are selected in the case of the vortex of pitch $3T_0$ and 1 turn, Fig. 9. As the topological charge is no longer an integer, the intensity field is no longer axisymmetric. As noted

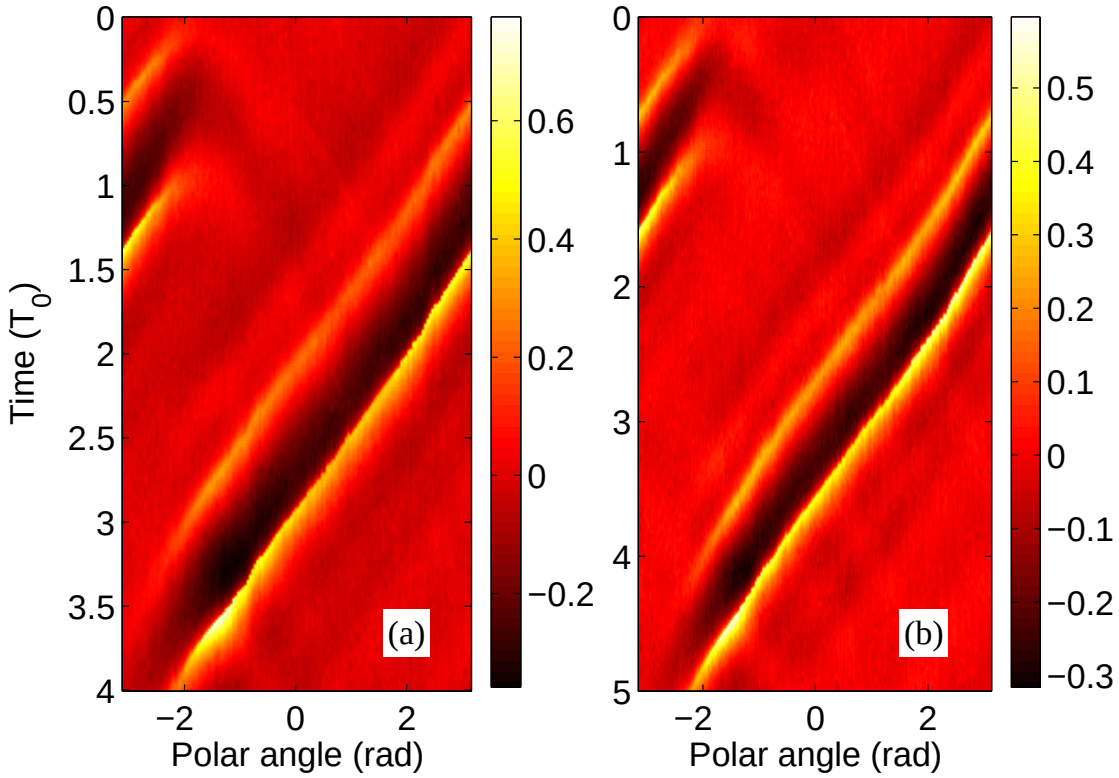

FIG. 8. (Color online) Pressure amplitude measured at $z = 600mm$ for transient vortices of pitch 3 T_0 (a) and 4 T_0 (b) on a ring of width $0.5mm$ and radius $12mm$ and $15mm$ respectively. The vortices are made of 1 turn.

before, for a fractional topological charge, the field is discontinuous at some θ value. Such a field contains evanescent components and the discontinuity is rapidly smoothed by diffraction localized at this θ value, see also the appendix for more mathematical details. A zero amplitude is observed as expected when the charge is half of an integer, 2.5 here ($\omega/\omega_0 = 2.5/3$), since the phase jump is π in this case. For this charge, in addition to the phase singularity of charge 2 in the vortex core, a second phase singularity is clearly visible but not at the center yet. It is located on the vortex "ring", where the amplitude vanishes. As the charge increases, this second phase singularity progressively migrates (see the case $\omega/\omega_0 = 2.75/3$) towards the center, while the ring of intensity is closing.

As in the previous section, the phase is extracted on the same large radius but now for five angular frequencies : $(l-1, l-0.75, l-0.5, l-0.25, l)/l\omega_0$. The phase for $\theta = -\pi$ has been subtracted so that the five curves start at the origin of the graph. The phase is linear with the polar angle on a large portion of the domain, as expected from Eq. 4. In this area the slopes are computed with a linear regression and these lines are plotted. The slopes are as expected equal to $l\omega/\omega_0$. However the total phase increment on a turn is quantized. This is possible thanks to the smooth transition between the two straight parts of the curve around $\theta = -2$. This smooth transition switches from a negative contribution to a positive one around $(l+0.5)/l\omega_0$ so that the total phase increment switches from $(l-1)2\pi$ to $l2\pi$. These results confirm the loss of the circular symmetry and the smooth transition induced by diffraction. The direction of the momentum is constant on a large angular sector far from the edges and in this area its azimuthal component is continuously adjustable with the helix pitch (the phase slope). If one is interested in orbital momentum transfer to absorbing particles or targets, the helix pitch is the important parameter.

These figures, phase slope, phase increment can be calculated as in the previous section, Tab. II, but now at each frequency, Fig. 11. The phase slope is a straight line as expected from Eq. 4. However the phase increment is quantized, Eq. 27, and takes the expected values. Whereas the computation with Eq. 25 is also nicely quantized but the levels are below the expected values for high frequencies obtained here by nonlinear harmonic pumping. This discrepancy may come from the experimental noise that increases artificially the energy.

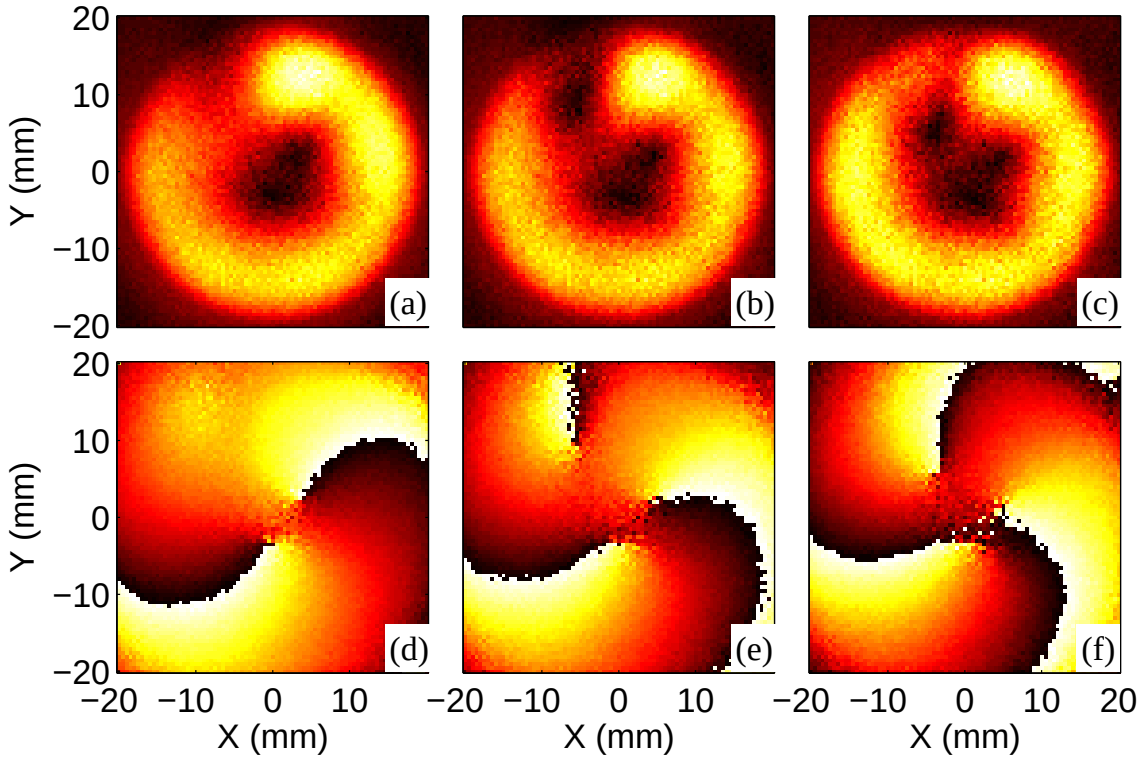

FIG. 9. (Color online) Modulus (subplots (a), (b) and (c)) and phase (subplots (d), (e) and (f)) of a vortex of pitch 3 T_0 and duration 1 turn measured at $z = 600mm$, at 3 angular frequencies located between two spectral lines of Fig. 4: $2.25/3\omega_0$ ((a) and (d)), $2.5/3\omega_0$ ((b) and (e)) and $2.75/3\omega_0$ ((c) and (f)).

E. The angular phase velocity

The energy velocity and phase velocity are identical in a isotropic and non dispersive medium. The energy velocity is defined as the ratio between the Poynting vector and the energy density and can be easily computed from the relation:

$$\vec{c^e} \cdot \vec{n} = c \tag{29}$$

and Eq. 3 so that:

$$\vec{c^e} = \omega \frac{\vec{k}}{\vec{k}^2}. \tag{30}$$

This yields the azimuthal energy velocity:

$$c_\theta^e = c \frac{l/(kr)}{\left((\varphi_{,r})^2 + (l/(kr))^2 + (\varphi_{,z})^2\right)}. \tag{31}$$

The new charge defined in Eq. 4 is introduced in Eq. 31 to get :

$$c_\theta^e = c \frac{l/(k_0 r)}{\left((\varphi_{,r})^2 + (l/(k_0 r))^2 + (\varphi_{,z})^2\right)}. \tag{32}$$

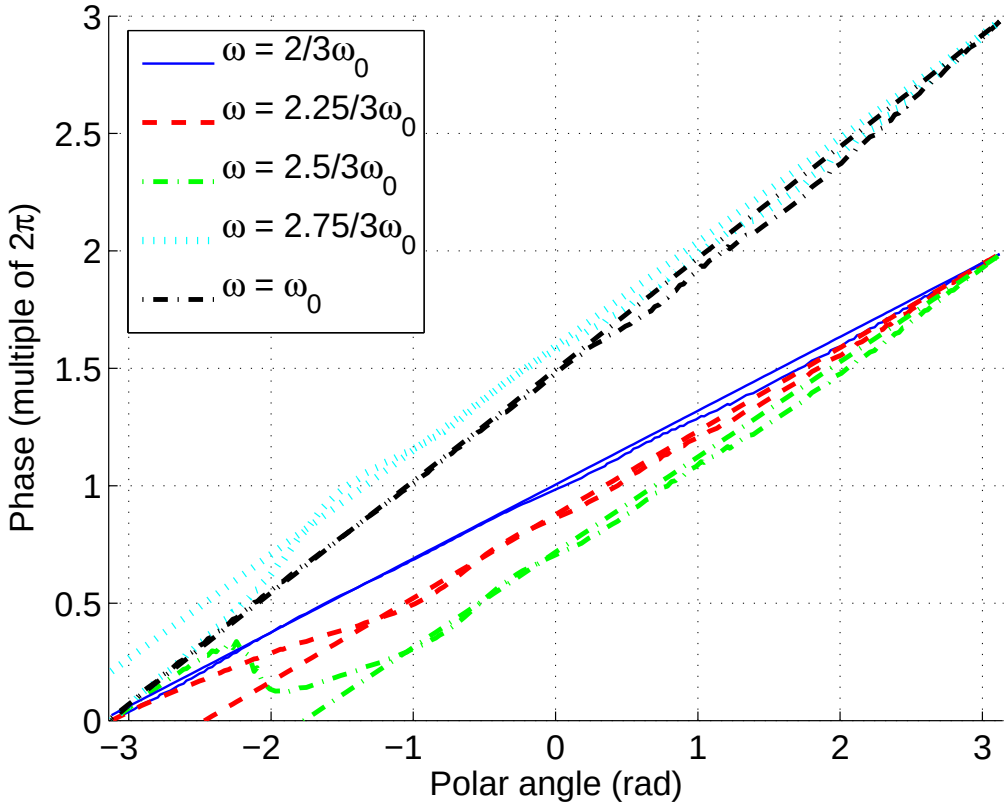

FIG. 10. (Color online) Phase measured at $z = 600mm$ for transient vortices of pitch 3 T_0 on a ring of width $0.5mm$ and radius $12mm$. 5 angular frequencies located at $2/3\omega_0$ (solid blue line), $2.25/3\omega_0$ (dashed red line), $2.5/3\omega_0$ (dashed-dotted green bottom line), $2.75/3\omega_0$ (dotted cyan line) and ω_0 (dashed-dotted black upper line) are plotted. The fitting lines obtained by linear regression are plotted with the same line types and colors.

where $k_0 = \omega_0/c$.

For a paraxial wave, one can check that this rotation is slow:

$$(\varphi_{,r})^2 \ll 1,\ (\varphi_{,z})^2 \approx 1, l/(k_0 r) = (l\lambda_0)/(2\pi r) \ll 1 \Rightarrow c_\theta^e \approx c\frac{l}{k_0 r} \ll c \tag{33}$$

Indeed, the phase of a vortex of order l varies of $2l\pi$ on a circular contour around its axis of length $2\pi r$. This variation in a transverse plane can be analyzed by angular spectrum decomposition. This plane wave decomposition introduces a transverse wavelength $\lambda_t = \lambda_0/\sin(\phi)$, where ϕ is the angle of the plane wave with the axis. ϕ is bounded by $\pi/2$ at evanescent cutoff where $2\pi r = l\lambda_t = l\lambda_0$. For radial coordinates closer to the axis the field intensity should be exponentially decreasing. A paraxial wave is made of plane waves whose directions of propagation are close to the beam axis: $\sin(\phi) \ll 1$ and hence we may restrict our analysis to $(l\lambda_0)/(2\pi r) \ll 1$.

We apply Eq. 33 to our vortex of pitch $3T_0$ in order to compute the angle of rotation, $\Delta\theta$, when the vortex propagates from $z = 450\ mm$ to $z = 600\ mm$. The computation is: $\Delta\theta = \left(c_p^\theta/r\right)(\Delta z/c)$ with $r \approx 15\ mm$, $c = 1470\ m.s^{-1}$, $\omega_0/2\pi = 1.1$ MHz and a distance $\Delta z = 150\ mm$. We get $\Delta\theta \approx 30$ degrees. Since for a fractional charge the field is not axi-symmetric, this azimuthal evolution can be used as a marker to determine the rotation of the helix during the propagation. On Fig. 12, the modulus (subplot (a)) and the phase (subplot (b)) are displayed for the vortex of pitch $3T_0$, 1 turn, $\omega = 2.5/3\omega_0$, and at distance $z = 450\ mm$. A comparison with Fig. 9 where the same beam is measured at $z = 600\ mm$ shows that indeed, the field has been rotated by an angle of about 30 degrees. However the accuracy of this measurement is poor, since the hole in the ring is significantly enlarged by diffraction at $z = 600\ mm$. Moreover the radial coordinate of the intensity ring is not measured with a good accuracy. Nevertheless the qualitative agreement is good. Note that the travel time is close to 100 T_0 since $\Delta z \approx 100\lambda_0$, which is very large compared to the helix pitch lT_0. This azimuthal velocity should not be confused with the rotation velocity when the time evolution of

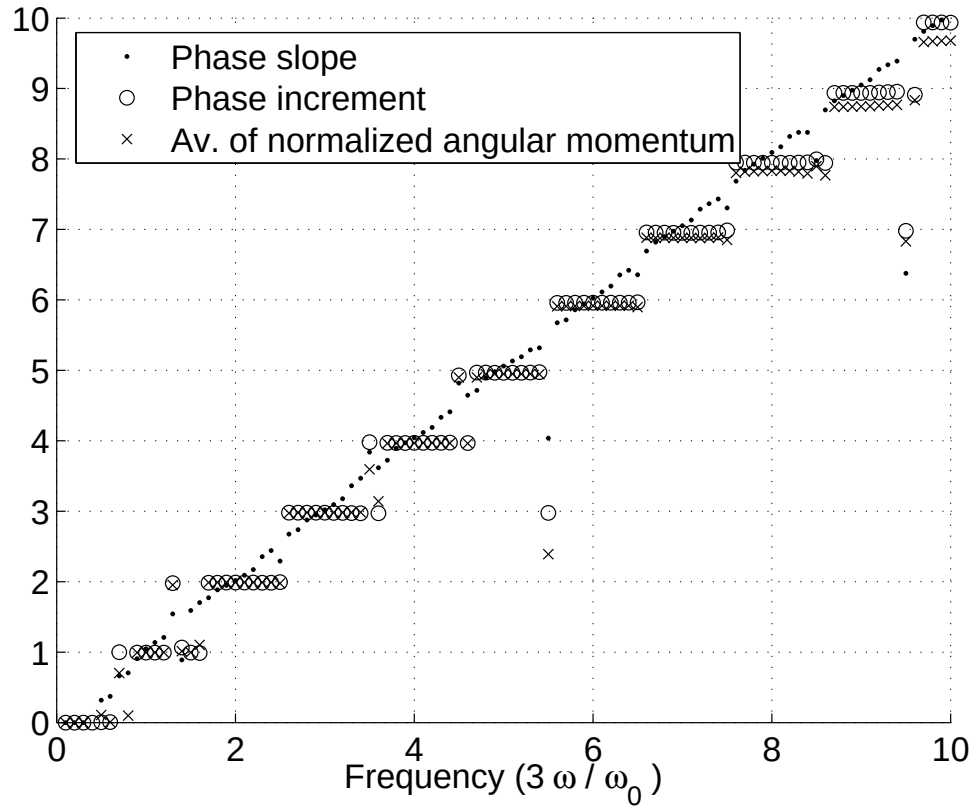

FIG. 11. Phase slope (dot), phase increment in multiple of 2π (Eq. 27 multiplied by ω, circle) and average of the normalized angular momentum (Eq. 25 multiplied by ω, cross).

the field is measured in a transverse plane, see [10]. In that last case, as demonstrated in part II, Eq. 8 and visible on Figs. 5, 8, a revolution is performed in a duration equal to the pitch lT_0.

F. Uncertainty relation

Another feature emphasized here is: the shorter the pulse, the higher the charge is and the more the pressure field is confined in a small angular sector of a cross-section plane at z and t fixed, Fig. 5. Thus a one period pulse will occupy a third of the circumference for a pitch $3T_0$ at a given time. This angular localization of the field at a given z and time t must be associated with a spreading of the angular momentum. This spreading appears in Eq. 10 and is experimentally confirmed by Fig. 4: the shorter the pulse, the larger its spectral width. However this spectral width determines the number of charges necessary to synthesize the vortex, that means the spreading of the angular momentum, Eq. 10. Note that this angular confinement of the field is due to the measurement onto a 2D transverse plane of the 3D wave field. Actually the field is invariant on a helix if the number of turns is infinite. This uncertainty principle between the angle position and the orbital angular momentum can be easily derived from the previous analysis. This remains valid for any scalar field. Indeed Eq. 22 implies:

$$\Delta\mathcal{M}_z = \frac{l}{\omega_0}\Delta\mathcal{E}, \tag{34}$$

whereas Eq. 8 or Eq. 11 for the continuous case provides a relation between standard deviation of polar angle and time:

$$\Delta\theta = \frac{\omega_0}{l}\Delta t. \tag{35}$$

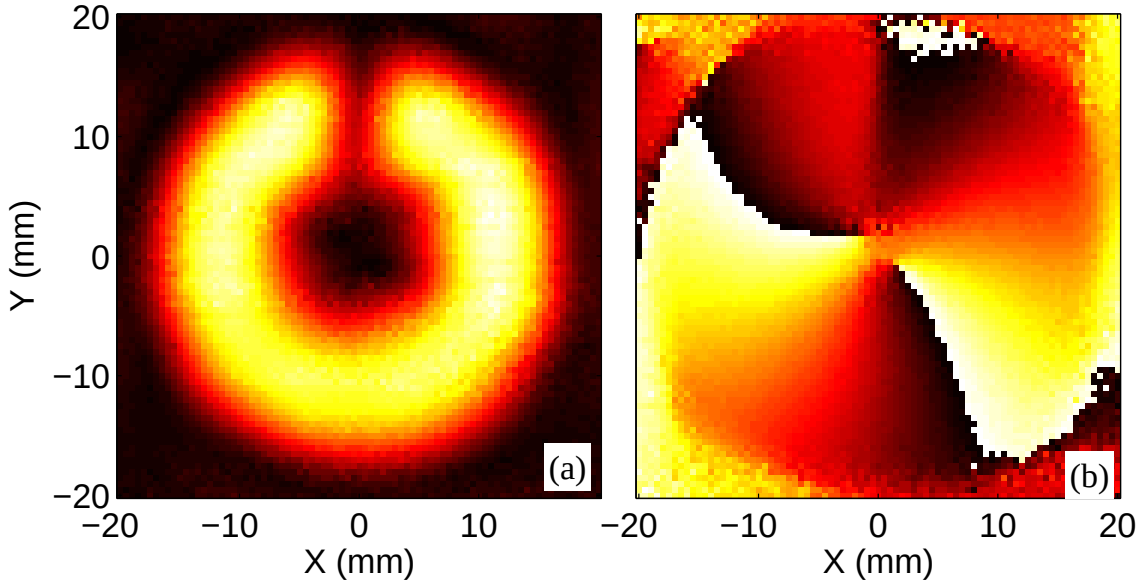

FIG. 12. (Color online) Modulus (a) and phase (b) of vortex of pitch 3 T_0 and duration 1 turn measured at $z = 450mm$. The angular frequency is located between two spectral lines of Fig. 4 at $2.5/3\omega_0$

Multiplying the two, we have the same uncertainty relation between angular momentum and polar angle on one side, as between energy and time on the other side:

$$\Delta\theta\Delta\mathcal{M}_z = \Delta t\Delta\mathcal{E}. \tag{36}$$

That last uncertainty relation between time and energy comes from the Fourier transform properties. Indeed the spectrum width of a pulse is inversely proportional to its duration. The pulse width in polar angle is the pulse duration multiplied by ω_0/l due to the projection of the helix onto the transverse plane, see Eq. 7. On the opposite, the orbital angular momentum is inversely proportional to ω_0/l since the Poynting vector component in the transverse plane is increasing with the pitch. This uncertainty principle occurs also if a monochromatic vortex is screened by an angular sector mask [26]. However here the angular dependence is not affected by the finite range of size 2π of the polar angle as soon as the elementary pulse time duration is shorter that the periodicity due to the helix pitch, lT_0. This limit corresponds to the existence or not of interferences between pulses attached to two consecutive turns. So for shorter pulses the angular position probability density is determined by the shape of the freely adjustable pulse envelope only. When the number of turns is large the energy distribution becomes confined to spectral lines due to the "orbital" resonances. However, even in this case, the spectral lines amplitudes are determined by the spectral width of the elementary pulse and the number of turns is responsible of the line-width, Eq. 12. Hence the uncertainty relation is unchanged but the standard deviation of the orbital angular momentum is now increasing by jump from one spectral line to the next one, whereas the standard deviation in angle remains a continuous function.

IV. DISCUSSION

A generalization of helicoidal waves, or vortices, for transient regimes has been derived for scalar wave fields. It shows that the pulse wavefront remains a half helicoid whatever the frequency, provided the definition of the charge is modified. This last one is a measurement of the stretching of the helix and this helix pitch is no longer quantized. This modification shows that the frequency components of the pulse vortex are monochromatic vortices of consecutive integer charges if the helix has an infinite number of turns. The number of observed charges is determined by the bandwidth of the elementary pulse and the helix pitch. This is in agreement with the uncertainty principle. Indeed as a shortening of the pulse implies a localization of the energy within a smaller angular sector, this must be accompanied

by a spreading of the angular momentum. Besides, a sharp truncation in the axial direction would lead to vortices with fractional charges at intermediate frequencies between the spectral lines. However fractional vortices are discontinuous function of the polar angle and this discontinuity is smoothed by diffraction. This diffraction occurs at the head and tail of the truncated helicoidal wavefront where the field intensity is no longer axisymmetric. Although, the orbital momentum is no longer quantized in this last case, the phase increment along a closed curved is still. These results have been confirmed by ultrasonic experiments in water, for which shock waves are used to identify the wavefront, but the theoretical results are of general validity for either optical or acoustical vortices.

In particular, there may be of special interest for ultra-short optical vortices with femto-second sources. Indeed, if the generalization presented here is not taken into account, the shape of the pulse cannot be maintained and will vary with the polar angle. This may be one of the cause involved in the pulse lengthening observed in recent experiments with ultra-short sources and cited in the introduction. Another interesting point is that if this modification is actually applied, the pulse should be repeated with the adequate periodicity as described on Fig. 4 and Eq. 8. Otherwise, vortices with a single turn are synthesized and hence diffraction is strong. However this generalization may considerably simplify the problem since only spectral lines are required to synthesize pulse vortices with an infinite number of turns. For instance our experiment and analysis provide the number of spectral lines, or synchronized continuous laser sources, required to synthesize a pulse of predefined duration. Thus, if the central angular frequency is ω_0, the bandwidth $\Delta\omega$ and the helix pitch l/ω_0, then the number of spectral lines is $\Delta n = l\Delta\omega/\omega_0$, Eq. 12. Since Δn depends only on the relative bandwidth (the ratio $\Delta\omega/\omega_0$), a pulse of 1 cycle requires about l spectral lines whatever the central frequency. Note that to separate two pulses, the helix pitch must be longer than the pulse duration and hence for the case considered above $l \geq 2$. Hence a 1 cycle pulse optical vortex with $l = 3$ requires three synchronized continuous lasers only. The relative weight and phase of the continuous sources will determine the pulse duration.

V. APPENDIX: VORTICES OF FRACTIONAL CHARGE AND DIFFRACTION

We consider separate variables solutions of Helmholtz equation in cylindrical coordinates. The angular spectrum method is used here to propagate the field in direction z. The radial and azimuthal dependency of the field in a transverse plane, t and z fixed is:

$$\Psi\left(r,\theta,z=0\right)=f\left(r\right)e^{i\alpha\theta} \tag{37}$$

A 2D Fourier transform on coordinates (x, y) of the transverse plane is used to compute the angular spectrum.

$$\mathcal{F}_{2D}\left[f\left(r\right)\exp\left(i\alpha\theta\right)\right]=\iint f\left(r\right)\exp\left(i\alpha\theta\right)\exp\left\{-i\left(q_x x+q_y y\right)\right\}dxdy \tag{38}$$

The Cartesian coordinates are then changed to polar coordinates:

$$\begin{cases} q_x = q\ \cos\left(\nu\right) \\ q_y = q\ \sin\left(\nu\right) \end{cases} \quad \begin{cases} x = r\ \cos\left(\theta\right) \\ y = r\ \sin\left(\theta\right) \end{cases} \tag{39}$$

Applying this change of variables to Eq. 38, leads to

$$\mathcal{F}_{2D}\left[f\left(r\right)\exp\left(i\alpha\theta\right)\right]=\int_0^\infty f\left(r\right)r\ dr\int_{-\pi}^{\pi}\exp\left\{i\left(\alpha\theta-qr\cos\left(\theta-\nu\right)\right)\right\}d\theta \tag{40}$$

Another change of variable will transform the integral on the polar angle into the definition of the Bessel function. Firstly, we rewrite, Eq. 40:

$$\mathcal{F}_{2D}\left[f\left(r\right)\exp(\,i\alpha\theta\,)\right]=\exp\left\{i\left(\alpha\nu-\frac{\pi}{2}\right)\right\}\int_0^\infty f\left(r\right)rdr\int_{-\pi}^{\pi}\exp\left\{-i\left(\alpha\left(\nu-\theta-\frac{\pi}{2}\right)-qr\sin\left(\nu-\theta-\frac{\pi}{2}\right)\right)\right\}d\theta \tag{41}$$

Secondly, we set $\zeta = qr$ and $\tau = \mu - \theta - \pi/2$, and in the case, $\alpha = l \in \mathbb{Z}$. Then the integral on the polar coordinates is the integral definition of the Bessel function:

$$\int_{-\pi}^{\pi}\exp\left\{-\left(il\tau-x\ \sin\left(\tau\right)\right)\right\}d\tau=2\pi J_l\left(\zeta\right) \tag{42}$$

since the integrand is a periodic function and the domain of integration is one period of this function. We can then rewrite the Fourier integral as a Hankel transform of order l of the function f, noted $\mathcal{H}_l[f](q)$:

$$\mathcal{F}_{2D}[f(r)\exp(il\theta)] = 2\pi\exp\left\{i\left(l\nu-\frac{\pi}{2}\right)\right\}\int_0^\infty f(r)\,J_l(qr)\,rdr = 2\pi\exp\left\{i\left(l\nu-\frac{\pi}{2}\right)\right\}\mathcal{H}_l[f(r)](q),\ l\in\mathbb{Z} \tag{43}$$

To go further, the function $f(r)$ must be defined. We are looking for solutions of the Helmholtz equation with separated variables. These solutions are well known since they are used to identify the modes of a cylindrical wave guide:

$$\psi(r,\theta,z,t) = J_l(\kappa r)\exp\{i(l\theta+k_z z-\omega t)\},\ \ \kappa^2+k_z^2=\left(\frac{\omega}{c}\right)^2,\ \ \kappa\neq 0 \tag{44}$$

The case $\kappa = 0$ is the case of the r-vortex, $f(r) = r^{\pm\alpha}$. In the following, we choose in Eq. 37, $f(r) = J_l(\kappa r)$, $\alpha = l \in \mathbb{Z}$ and $z = 0$. Then the field can be easily propagated with the angular spectrum method at range z using the orthogonal relation of Bessel function:

$$\mathcal{H}_l[J_l(\kappa r)](q) = \frac{\delta(\kappa-q)}{\kappa} \tag{45}$$

so that the angular spectrum of this field is a ring of radius $q = \kappa$ and hence contains no evanescent waves as long as $\kappa \leq \omega/c$. The field propagated at an arbitrary range z writes:

$$\mathcal{F}_{2D}^{-1}[\mathcal{F}_{2D}[\psi(r,\theta,0,t)]\exp(imz)] = \psi(r,\theta,z,t),\ \ m=\sqrt{\left(\frac{\omega}{c}\right)^2-q^2} \tag{46}$$

This result is rather trivial since on the one hand, $\psi(r,\theta,z,t)$ is a well known valid solution of the Helmholtz equation with separated variables and on the other hand, the dependence on z, $k_z z - \omega t$, corresponds to the time of flight. On the contrary if $l = \alpha \notin \mathbb{Z}$ in Eq. 44, the field is no longer a continuous function of the polar angle, see Eq. 2. This means that ψ is not actually a solution of the homogeneous Helmholtz equation. Indeed, it is a solution of the inhomogeneous Helmholtz equation. A source term involving distributions is required to take into account the partial derivatives of the discontinuity at $\theta = \pm\pi$. The same problem arises for Green function. For instance in 2D or cylindrical coordinates, Bessel functions of the third kind, or Hankel functions are solution of an inhomogeneous Helmholtz equation with a divergence on the axis. The angular spectrum of the Hankel functions contains evanescent components. Their sum the Bessel function is a regular function. Even if a Bessel wave of fractional order is not a valid solution of the homogeneous Helmholtz equation, it can be used as boundary condition at $z = 0$. This boundary condition may be propagated with the angular spectrum method. However, in the previous derivation, if $l \notin \mathbb{Z}$ then the integral on the left hand-side of Eq. 42 is not a Bessel function. Therefore the previous derivation is no longer valid. We may decompose the azimuthal dependence as a Fourier series:

$$\exp(i\alpha\theta) = \sum_{n=-\infty}^{\infty}\frac{\sin(\pi(\alpha-n))}{\pi(\alpha-n)}\exp(in\theta) \tag{47}$$

Using Eq. 47 in Eq. 41 and using again the Bessel function definition, Eq. 42 gives a new equation comparable to Eq. 43:

$$\mathcal{F}_{2D}[f(r)\exp(i\alpha\theta)] = 2\pi\exp\left(-i\frac{\pi}{2}\right)\sum_{n=-\infty}^{\infty}\frac{\sin(\pi(\alpha-n))}{\pi(\alpha-n)}\exp(in\nu)\,\mathcal{H}_n[f(r)](q),\ \alpha\in\mathbb{R} \tag{48}$$

As separated variables solutions of the Helmholtz equation involve the solution of the Bessel equation for radial dependence, therefore the general solutions is written as in Eq. 44, but now the integer azimuthal index l is replaced by $\alpha \in \mathbb{R}$. More generally the radial dependence can be written as a sum of Bessel waves of order α with varying κ:

$$f(r) = \int_0^{\omega/c}\left[A(\kappa)J_\alpha(\kappa r)+B(\kappa)J_{-\alpha}(\kappa r)\right]d\kappa \tag{49}$$

since J_α and $J_{-\alpha}$ are two independent solutions of the Bessel equations if $\alpha \notin \mathbb{Z}$. The interval of integration is bounded by ω/c to reject evanescent waves, see Eq. 44. The derivation used for the integer case breaks because we can no longer use the orthogonal relation, Eq. 45. Indeed the $\mathcal{H}$ involves now two Bessel functions of different orders: n and α. Hence calculating Eq. 46 is much more difficult and requires numerical solutions.

However we may use the angular spectrum propagator to get the field at z:

$$\psi(r,\theta,z) = \mathcal{F}_{2D}^{-1}\left[\mathcal{F}_{2D}\left[f\left(r\right)\exp\left(i\alpha\theta\right)\right]\exp\left(imz\right)\right] \tag{50}$$

and get:

$$\psi(r,\theta,z) = 2\pi\exp\left(-i\frac{\pi}{2}\right)\sum_{n=-\infty}^{\infty}\frac{\sin\left(\pi\left(\alpha-n\right)\right)}{\pi\left(\alpha-n\right)}\frac{1}{\left(2\pi\right)^2}\iint\mathcal{H}_n\left[f\left(r\right)\right]\left(q\right)\exp\left(in\nu\right)\exp\left\{i\left(q_x x+q_y y\right)\right\}dq_x dq_y \tag{51}$$

Performing the same change of variable from Cartesian to polar coordinates yields:

$$\psi(r,\theta,z) = \sum_{n=-\infty}^{\infty}\frac{\sin\left(\pi\left(\alpha-n\right)\right)}{\pi\left(\alpha-n\right)}\exp\left(in\theta\right)\int_0^{\omega/c}\mathcal{H}_n\left[f\left(r\right)\right]\left(q\right)\exp\left(imz\right)J_n\left(rq\right)qdq \tag{52}$$

Since the Fourier series is unique, the field is non diffracting if and only if:

$$\forall z,\ \forall n,\ \int_0^{\omega/c}\mathcal{H}_n\left[f\left(r\right)\right]\left(q\right)\exp\left(imz\right)J_n\left(rq\right)qdq = f(r)\exp\left(ik_z z\right) \tag{53}$$

which is obviously not true. And it is also clear that the field is no longer a function with separated variables as expected since this field is a solution of an inhomogeneous Helmholtz equation. Reciprocally, the modeling of the ends of the helicoidal wavefront requires both diffraction and a coupling between the coordinates (r,θ,z) that can not be described by integer topological charges.

---

[1] J. F. Nye and M. V. Berry, Proc. R. Soc. Lond. A. **336**, 165 (1974).
[2] L. Allen, M. W. Beijersbergen, R. J. C. Spreeuw, and J. P. Woerdman, Phys. Rev. A **45**, 8185 (1992).
[3] G. Molina-Terriza, J. P. Torres, and L. Torner, Phys. Rev. Lett. **88**, 013601 (2001).
[4] A. Vaziri, G. Weihs, and A. Zeilinger, Phys. Rev. Lett. **89**, 240401 (2002).
[5] A. Mair, A. Vaziri, G. Weihs, and A. Zeilinger, Nature **412**, 313 (2001).
[6] H. He, M. E. J. Friese, N. R. Heckenberg, and H. Rubinsztein-Dunlop, J. Mod. Optics **42**, 217 (1995).
[7] B. T. Hefner and P. L. Marston, J. Acoust. Soc. Am. **106**, 3313 (1999).
[8] J.-L. Thomas and R. Marchiano, Phys. Rev. Lett. **91**, 244302 (2003).
[9] R. Marchiano, F. Coulouvrat, L. Ganjehi, and J.-L. Thomas, Physical Review E **77**, 016605 (2008).
[10] T. Brunet, J.-L. Thomas, R. Marchiano, and F. Coulouvrat, New J. Phys. **11**, 013002 (January 2009).
[11] R. Marchiano and J.-L. Thomas, Phys. Rev. Letters **101**, 064301 (2008).
[12] K. Volke-Sepulveda, A. O. Santillan, and R. R. Boullosa, Phys. Rev. Lett. **100**, 024302 (January 2008).
[13] K. Bezuhanov, A. Dreischuh, G. G. Paulus, M. G. Schätzel, and H. Walther, Opt. Lett. **29**, 1942 (2004).
[14] I. Mariyenko, J. Strohaber, and C. Uiterwaal, Opt. Express **13**, 7599 (2005).
[15] I. Zeylikovich, H. I. Sztul, V. Kartazaev, T. Le, and R. R. Alfano, Opt. Lett. **32**, 2025 (2007).
[16] A. Schwarz and W. Rudolph, Opt. Lett. **33**, 2970 (2008).
[17] A. J. Wright, J. M. Girkin, G. M. Gibson, J. Leach, and M. J. Padgett, Opt. Express **16**, 9495 (2008).
[18] J. Durnin, J. Opt. Soc. Am. A **4**, 651 (1987).
[19] J.-Y. Lu and J. Greenleaf, IEEE Trans. Ultrason., Ferroelec., Freq. Cont. **39**, 19 (1992).
[20] M. V. Berry, J. Opt. A: Pure Appl. Opt. **6**, 259 (2004).
[21] J. C. Gutiérrez-Vega and C. López-Mariscal, J. Opt. A: Pure Appl. Opt. **10**, 015009 (2008).
[22] J. Leach, E. Yao, and M. J. Padgett, New J. Phys. **6**, 71 (July 2004).
[23] P. L. Overfelt, Phys. Rev. A **46**, 3516 (Sep 1992).
[24] K. Dholakia, N. B. Simpson, M. J. Padgett, and L. Allen, Phys. Rev. A **54**, R3742 (1996).
[25] R. Marchiano, J.-L. Thomas, and F. Coulouvrat, Phys. Rev. Let. **91(18)**, 184301(1 (2003).
[26] S. Franke-Arnold, S. M. Barnett, E. Yao, J. Leach, J. Courtial, and M. Padgett, New J. Phys. **6**, 103 (2004).